

Synthesis and Biomedical Application of SiO₂/Au Nanofluid Based on Laser-Induced Surface Plasmon Resonance Thermal Effect

Mohammad E. Khosroshahi*, Mohammad Sadegh Nourbakhsh, Lida Ghazanfari

Faculty of Biomedical Engineering, Biomaterials Group,

Laser and Nanobiophotonics Lab., Amirkabir University of Technology, Tehran, Iran

*E-mail: *khosro@aut.ac.ir*

Received September 18, 2010; revised March 26, 2011; accepted April 15, 2011

Abstract

We described the synthesis of Au coated SiO₂ nanoshells linked with NH₂ biomolecular ligands using a simple wet chemical method with a particular application for laser tissue soldering. Tunable nanoshells were prepared by using different gold colloidal concentrations. The nanoshells are characterized by UV-vis spectroscopy, FTIR, XRD and AFM. The FTIR results confirmed the functionalized surfaces of silica nanoparticles with NH₂ terminal groups. A broad absorption was observed between 470 - 600 nm with a maximum range between 530 - 560 nm. Based on the XRD results three main peaks of Au (111), (200) and (220) were identified. In addition, AFM results showed that the diameter of silica core was between 90 - 110 nm with gold shell thickness between 10 - 30 nm. A possible tissue soldering using gold nanoshells and laser-induced thermal effect based on surface plasmon resonance is demonstrated. In our case this corresponds to 90°C (*i.e.* below vaporization) using the higher gold concentration (2 ml) at 60 W·cm⁻².

Keywords: Gold Nanoshells, Synthesis, UV-vis Spectroscopy, XRD, AFM, Tissue Soldering PACS 44.40 + a, 78.20.-n, 78.20.nb

1. Introduction

Plasmonic materials have been used for at least 1700 years, although it is believed that those days craftsman did certainly not understand the physics behind them. But one of the oldest and glamorous plasmonic glass materials is the “Lycurgus” cup from the fourth century A.D. which appears red when transilluminated, but shines green when imaged in reflection. Basically a nanoshell is a type of spherical nanoparticles consisting of a dielectric core which is covered by a thin metallic shell. A nanoshell involves plasmon which essentially is a collective excitation or quantum plasma oscillation where the electrons simultaneously oscillate with respect to all the ions. The interaction of light and nanoparticles affects the displacement of charges which in turn affects the coupling strength. Such nanoparticles exhibit strong optical scattering and absorption at above region due to localized surface plasmon resonance (LSPR). This is a classical effect in which the light’s electromagnetic field drives the collective oscillation of the nanoparticles free

electrons into resonance. The resonance is the effect of maximum oscillation amplitude at particular frequency. The subject was theoretically described by Mie in 1906 by solving Maxwell equations for a metal sphere surrounded by a dielectric medium using the dielectric function of the bulk metal [1-3]. Gold nanoshells exhibit strong absorbance with tunable wave length in the NIR region where effectively converts the light energy into heat. But one major common disadvantage in biomedical applications is the lethal over dose of radiation as a side effect and hence increasing the chance of damaging surrounding healthy tissue. However, one possible practical approach would be to use NIR light due to lack of absorption by tissue component and LSPR because the increase in the magnitude of the oscillations effectively converts the light energy into heat. In this respect, not only gold seems very useful but also due to its superior physic-chemical properties *e.g.*: corrosion resistant, low toxicity, conformational flexibility which all make this noble metal very attractive for biomedical applications [4,5]. It worth to notice that gold nanoshells have similar

properties to gold nanoparticles but with the added benefit of being tunable to different wavelengths, using different thickness. Also they are more efficient in converting EM waves to energy than nanoparticles. This is due to plasmon resonance along both the inner and the outer surfaces of the shell, as opposed to nanoparticles only having resonances along the outer surface. In fluids, considerable attention has been devoted to the so called nanofluids [6,7], in which nanoparticles in dilute suspension appear to modify both bulk heat transfer and critical heat fluxes. Generally nanofluids are formed by dispersing nanometer-sized particles (1 - 100 nm) or droplets in heat transfer fluids. Nanoparticles have unique properties, such as large surface area to volume ratio, dimension-dependent physical properties and lower kinetic energy which can be exploited by the nanofluids [8]. At the same time, the large surface area makes nanoparticles better and more stably dispersed in base fluids. Compared with micro-fluids or mili-fluids, nanofluids stay more stable, so they are promising for many practical applications such as in medicine and clinical engineering. In this work, we report the synthesis, characterization and application of binary SiO₂/Au nanofluids with different concentrations for tissue soldering based on LSPR.

2. Theory

2.1. E.M.W-Metal Interaction

Basically, the rationales behind the metallic core-shell nanofluid lies in the following steps: field coupling, displacement of charges, dielectric polarization (*i.e.* electric dipole moment) and harmonic oscillator. Let us assume the total energy (u) of a electromagnetic field is obtained by integration over the corresponding volume (V) of spherical nanoparticles,

$$u = \varepsilon_0 \int_V |\underline{E}(r)|^2 d^3r \quad (1)$$

where an oscillating photon with frequency ω has energy $u = \hbar\omega$. One can get the average field strength $\langle |E| \rangle = \sqrt{\hbar\omega / \varepsilon_0 V}$ that corresponds to one photon. This quantity is important if for example one wants to describe the coupling of particle to the field oscillation. For monochromatic planar waves the characteristic solution of the Helmholtz equation is

$$(\nabla^2 + k^2)\underline{E}(r) = 0 \quad (2)$$

in Cartesian coordinate (x, y, z): and these waves are vector waves with constant polarization vector ε and amplitude E_0 ,

$$\underline{E}(r, t) = \text{Re}[E_0 \varepsilon e^{-i(\omega t - kr)}] \quad (3)$$

we define the wave vector by $k \cdot r = \text{constant}$ where r is the distance and planes with phase $\Phi = \omega t - kr$. Now, in conducting materials (such as Au shell in our case) charges can be move freely but under influence of an applied external time varying electric field (e.g. laser) accelerate electrically charged particles and in doing so it generates polarization and current through displacement of charges. Thus by using Maxwell's equation for time varying fields, we get

$$\nabla \times \underline{H} = j + \frac{\partial}{\partial t} D \quad (4)$$

where D is dielectric displacement given by $\frac{\partial}{\partial t} D = j_{dis} + j_{pol}$ with j_{dis} and j_{pol} are displacement and polarization currents respectively. Also we know that the polarization charge is defined as

$$P = \underline{E} \chi \quad (5)$$

where χ the optical susceptibility is a constant. If the polarization is proportional to the electric field, χ is "linear" (*i.e.* χ^1), if not then the relation become non-linear" (*i.e.* χ^2, χ^3). When the polarization significantly increases with increasing \underline{E} , the property used for special functions such as oscillators.

2.2. Core-Shell Nanoparticle Plasmons Resonance

The conduction band electrons in metals can undergo a coherent oscillation, the so-called plasma oscillation. The electromagnetic field of the incoming light wave can induce polarization of the conduction electron which means the electrons are displaced with respect to the heavier positive core ions. The dielectric response of a metal to electromagnetic radiation is given by the complex dielectric constant,

$$k_{sp} = \frac{\omega}{c} \sqrt{\frac{\varepsilon_c \varepsilon_m}{\varepsilon_c + \varepsilon_m}} \quad (6)$$

where k_{sp} is the surface plasmon wave vector, ω is the frequency of light and $\varepsilon_c, \varepsilon_m$ represent the dielectric of core (SiO₂) and Au respectively. It should be noted that ε_c is the (purely real) dielectric constant, and $\varepsilon_m = \varepsilon_r + j\varepsilon_i$ is the complex dielectric constant of the metallic nanoparticles. The real part (ε_r) determines the degree to which the metal polarizes in response to an applied external electric field and the imaginary part, $j\varepsilon_i$, quantifies the relative phase shift of this induced polarization with respect to the external field and it include losses (e.g. ohmic loss as heat). An important quantity in a metal dielectric response is the plasmon frequency defined as

$$\omega_p^2 = \frac{n_e e^2}{m_{eff} \epsilon_0} \quad (7)$$

where n_e is the density of electrons, e is the electron charge (1.6×10^{-19} C) and ϵ_0 is the vacuum dielectric constant permittivity (8.85×10^{-12} Fm⁻¹). We know that the dimensions of metallic nanoparticles are so small that light can easily penetrate the whole nanoparticle (unlike the thin-film interface) and grasp at all conduction band electrons. The result is that the sea of conduction band electrons is displaced with respect to positively charged ions from the metallic lattice. The resulting electric dipole on the particle represents a storing force and hence the nanoparticle can be considered as harmonic oscillator, driven by a light wave and damped by some ohmic losses e.g. heat as radiative (scattering) losses. The latter is equivalent to the re-emission of photon on the expense of nanoparticle plasmon (NPP) excitation. Since the NPPs are localized, we do not have to worry about wave vectors in their excitation. We can always excite a spherical metal NPP regardless of the incident radiation direction. The only needed condition is to choose the correct wavelength [9].

2.3. Harmonic Oscillators

The interaction of *e.m.w* radiation with polarizable matter goes back to H.Lorentz. In his model, electrons are considered that are harmonically bound to an ionic core with a spring (*i.e.* oscillatory atomic bond) and oscillating at optical frequencies ω_0 . The restoring force, $F_r = -m\omega_0^2 x$ and by assuming that damping of the oscillator is caused by release of the radiation energy, the damping force given by $F_d = -m\gamma(\frac{dx}{dt})$ where γ is the damping rate and $\gamma \ll \omega_0$. For simplification, we use complex quantities to write the orbit radius, $x \rightarrow r = x + iy$ thus we have,

$$\ddot{r} + \gamma\dot{r} + \omega_0^2 r = \frac{q}{m} \underline{E} e^{-i\omega t} \quad (8)$$

where $\underline{E} e^{-i\omega t}$ is the driving light-field. With the trial function $r(t) = \rho(t) e^{-i\omega t}$, the equilibrium solution $\rho(t) = \rho_0 =$ constant and

$$\rho_0 = \frac{qE/m}{(\omega_0^2 - \omega^2) - i\omega\gamma} \quad (9)$$

After some substitution and simplification one can get,

$$r(t) = x + iy = \rho_{max} \frac{\gamma}{2} \frac{\delta - i\gamma/2}{\delta^2 + (\gamma/2)^2} e^{-i\omega t} \quad (10)$$

in terms of the propagation of light in polarizable matter,

x and y give exactly the “dispersive” (x) and “absorptive” (y) components of the radiation interaction. It is known that an accelerated charge radiates and so a charged harmonic oscillator has to lose energy.

3. Materials and Methods

Hydrogen tetrachloraurate (HAuCl₄) (99.9%), tetraethylortosilicate (TEOS) (99.9%), 3-aminopropyltrimethoxysilane (APTMS), Tetrakis hydroxymethyl phosphonim chloride (THPC) (80% solution in water), Potassium carbonate (99%), formaldehyde, ammonium hydroxide solution (33% NH₃) and ethanol (99%), HPLC grade water and Sodium Hydroxide (99%) were obtained from Sigma-Aldrich Co. Silica nanoparticles prepared using following method: 3 ml of ammonia was first added to 50 ml of absolute ethanol, and then the mixture was stirred vigorously for 15 minutes. Different amounts (1 ml (sample A), 1.5 ml (sample B)) of TEOS were added to the mixture drop wise. For the concentration used here, the induction period was approximately 45 minutes after which the solution colour became cloudy as silica nanoparticles were grown and eventually turned to an opaque white solution. 25 μ L of APTMS was then added to 50 ml of the vigorously stirred silica nanoparticles solution and allowed to react for 2 hour. The functionalization reaction could be verified by stopping the stirring and observing the separation of the mixture to two layers: the APTMS-coated nanosilica particles precipitated at the bottom of the reactor and a clear solution remained at the top. The APTMS coated silica nanoparticles were purified at three different centrifuge speeds (2000, 3500 and 5500 rpm) for optimization purpose and then re-dispersed in ethanol.

For preparation of colloidal gold nanoparticles, 0.5 ml of 1 M NaOH and 1 ml of THPC solution (prepared by adding 12 μ L of 80% THPC to 1 ml of HPLC grade water) were added to a 45 ml of HPLC grade water. The solution was then stirred for 5 minutes. After this process 2 ml of 1% HAuCl₄ in water was added to the stirred solution. THPC gold solution preparation produced a brown colour solution within a few seconds after addition of chloroauric acid.

For attachment of colloidal gold to nanosilica particles, 1ml of APTMS-functionalized nanosilica particles dispersed in ethanol was added to 10 ml of gold colloid ($\sim 7 \times 10^{14}$ particles/ml) in a tube. The tube was shaken for 5 minutes and then was left to settle down for 2 hour. The mixture was subsequently centrifuged at 2000 rpm and a red colour pellet precipitated at the bottom of the tube. The supernatant was removed and the remaining red-colour pellet redispersed in HPLC grade water. The purified Au/APTMS/nanosilica particles then redispersed in

5 ml of HPLC grade water.

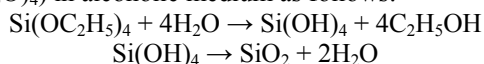
For growing the gold over the silica/APTMS/Au nanoparticles, 25 mg of potassium carbonate was dissolved in 100 ml water. After 10 minutes of stirring, 1.5 ml of 1% HAuCl₄ was added. This solution was initially yellow and after 30 minutes became colourless. 0.5 ml of the solution containing Au/APTMS/nanosilica was added to the colourless solution. After addition of 20 µL of formaldehyde the colourless solution became purple. The nanoshells were centrifuged and re-dispersed in HPLC grade water for preparation of final product.

The ultraviolet/visible (UV/visible) extinction spectra of the nanoparticles were measured in solution using the UV/VIS-spectrophotometer (Philips PU 8620) in the wavelength range of 190 to 900 nm with the appropriate mixture of ethanol and water as a reference. Solution spectra were obtained by measuring the absorption of a dilute solution in a cell with a path length of 10 mm. The synthesized silica, precursor seed particles and gold nanoshells at different stages of shell growth was imaged under the transmission electron microscopy TEM (Philips CM-200-FEG) operating at 120 kV. Samples were prepared by placing a drop of solution on a carbon coated copper grid and allowing the grid to dry on filter paper. The surface topography and roughness as well as the size of nanoshells were studied by atomic force microscopy (AFM) (Dual scope/Raster scope C26, DME, Denmark). Mid-infrared spectra of absorbance peaks of SiO₂, APTMS/Silica and Au/APTMS/SiO₂ were obtained by transmission mode of Fourier Transform infrared (FTIR; Bruker, EQUINOX 55, Germany).

4. Results and Discussion

4.1. Core-Shell Formation Procedure

Silica (SiO₂) is a popular material to form core shell particles because of its extraordinary stability against coagulation. Its non-coagulating nature is due to very low value of Hamaker constant, which defines the Van der Waal forces of attraction among the particles and the medium [10]. It is also chemically inert, optically transparent and does not affect redox reactions at core surfaces [11,12]. For various purposes it is desirable that particles remain well dispersed in the medium which can be achieved by suitably coating them to form an encapsulating shell. It is worth mentioning that the synthesizing SiO₂ nanoparticles may take place via the procedure developed by Stober *et al.* [13] This method involves hydrolysis and successive condensation of TEOS (Si (C₂H₅O)₄) in alcoholic medium as follows:



The adsorption of gold colloids on the silica cores is done by functionalizing their surface by APTMS with amino groups having positive zeta potentials. The attachment is basically achieved through electrostatic attraction between the aminated silica nanoparticles and the gold colloids having negative charges. A TEM was used to study the gold formation around silica core. Small colloids of gold particles are attached to APTMS—functionalized silica nanoparticles core which were then used to template the growth of gold over layer.

4.2. Morphological Analysis

Generally, by varying the relative ratio of TEOS to solvent one could synthesize the particles in various size. Here, the silica particles synthesized by this procedure were amorphous and porous and decrease in TEOS concentration led to the formation of smaller particles. The effect of centrifuge speed and the amount of TEOS on the diameter of silica core is shown in **Figure 1**. As it can be seen the core diameter increases with increasing the amount of TEOS and decreasing the centrifuge speed which effectively controls the agglomeration state.

The TEM images of SiO₂ (2a), SiO₂/APTMS/Au (2b) are shown in **Figure 2**. It is clearly seen that the SiO₂/APTMS/Au samples exhibit a relatively random size and distribution of gold seeds with a variable size between 10 - 30 nm which is much larger than the mean particle size of the THPC-induced gold colloids.

Figure 3(a) shows an AFM image of functionalized silica nanoparticles (~100 nm) synthesized by the procedure described earlier in the material and methods section. A 3-D image of the surface morphology indicating its roughness variation is shown in **Figure 3(b)**. An example of Au coated SiO₂ nanoshells and its 3-D image are respectively shown in **Figures 3(c)** and **(d)**. The size of the

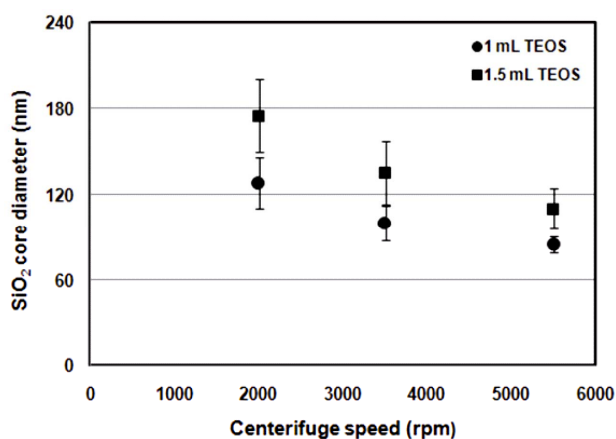


Figure 1. Effect of Centrifuge speed on the silica core diameter at constant TEOS concentration.

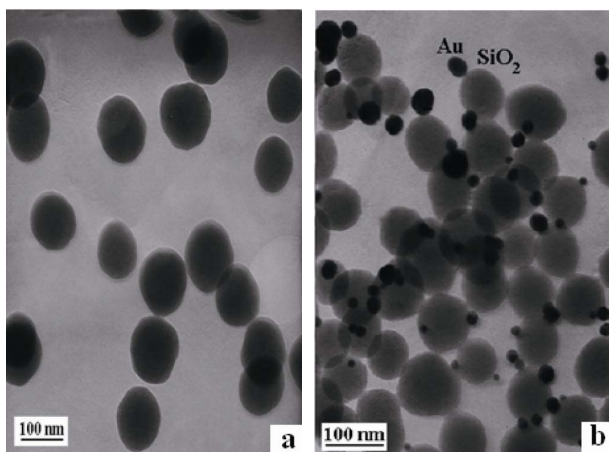


Figure 2. TEM images of the SiO₂ (a), Au-APTMS/SiO₂ and gold nanoshells samples (b) using 1ml TEOS.

nanoshells determined from AFM ranged between 90 and 110 nm. Surface roughness of SiO₂/Au nanoshells is calculated as 13 nm using SPM software. These images provided useful information about surface topography and the size of gold nanoparticles with well defined clarity, which effectively is correlated to optical absorption spectra.

4.3. Structural Analysis

Infrared spectroscopy offers a wealth of information regarding the structure of the surface of the nanoparticles. In particular, IR spectroscopy affords insight into the order and packing of the surface chains. The surface of the core particles is often modified with bi-functional molecules to enhance coverage of shell material on their surfaces [14,15]. The surface of core particles e.g. silica can be modified using bi-functional organic molecules such as APTMS. This molecule has a methoxy group at one end, and NH group at the other end. APTMS forms a covalent bond with silica particles through the OH group and their surface becomes NH-terminated. The FTIR spectra of SiO₂ functionalized with APTMS and gold coated nanoparticles for samples A and B are shown in **Figures 4** and **5**. The main peaks are 3431 cm⁻¹ (NH₂ asymmetric stretch), 1634 cm⁻¹ (O-H bending) and 466 cm⁻¹ for Si-O-Si bending mode. The shells showed Si-O-Si symmetric stretching at 801 cm⁻¹ and characteristic Si-O-Si asymmetric stretching at around 1100 cm⁻¹ respectively [16-18].

The particle phase analysis was performed by X-ray diffraction (XRD). The XRD pattern of nanoshells shown in **Figure 6** shows characteristic reflections of fcc gold planes (No. 04-0784). The diffraction features appearing at $2\theta = 38.20^\circ$, 44.41° , and 64.54° corresponds to the (111), (200) and (220) planes of the standard cubic

phase of Au respectively.

4.4. Optical Properties

UV-visible spectra recorded for two different samples are shown in **Figure 7**. For gold nanoparticles synthesized by 1ml TEOS, a peak was observed at about 535 nm. However, when 1.5 ml was used the peak was shifted to 556 nm. The resonance peak position depends on the plasmon interaction between separate inner and outer gold layers and the core-shell thickness. The addition of TEOS can efficiently cause the optical plasmon peaks to undergo a red-shift, which is consistent with the theoretical predictions of optical properties of metal coated particles given below:

$$\sigma_{ext} = \frac{9 \cdot V \cdot \epsilon_e^{3/2}}{c} \left(\frac{\omega \cdot \epsilon_i(\omega)}{[\epsilon_r(\omega) + 2\epsilon_e]^2 + \epsilon_i(\omega)^2} \right) \quad (11)$$

where V is the particle volume, ω is the angular frequency of the exciting light, and c is the speed of light. ϵ_e and $\epsilon_m(\omega) = \epsilon_r(\omega) + j\epsilon_i(\omega)$ are the dielectric functions of the embedding medium and the metal, respectively. The peak broadening is similar to the results observed by Wiesner [19] in spectroscopic studies of gold platelets in solution. In their case, the growing silica layer began to coalesce and encapsulated by different amounts of gold nanoparticles. Furthermore, the complete synthesized nanoshells, whose optical plasmon resonance peak ranges in the 500 - 600 nm regions can be used as a powerful tool in bio-imaging and bio sensing applications. The optical absorption spectra shown in **Figure 7** are relatively broad compared with that of pure gold colloid. The differences in peak positions and absorption intensities were caused by the cluster sizes of the deposited gold seeds on the silica nanoparticles, *i.e.*, the stronger plasmon resonance was caused by larger-sized gold clusters [20,21].

According to Mie scattering theory, the nanoshells geometry can quantitatively accounts for the observed plasmon resonance shifts and line-widths. In addition, the plasmon line-width is dominated by surface electron scattering [22,23]. The optical absorption of nanoshells varies according to core-shell diameter. For smaller size the peak shifts towards the shorter wavelength (blue shift) and for longer size it shows a red shift.

4.5. Modelling

The numerical results are shown in **Figure 8**. Calculations of the optical absorption of silica-gold nanoshells were performed by using a computer code employing Mie scattering for concentric sphere geometry. The required parameters are the core and shell radii, R_1 and R_2 ,

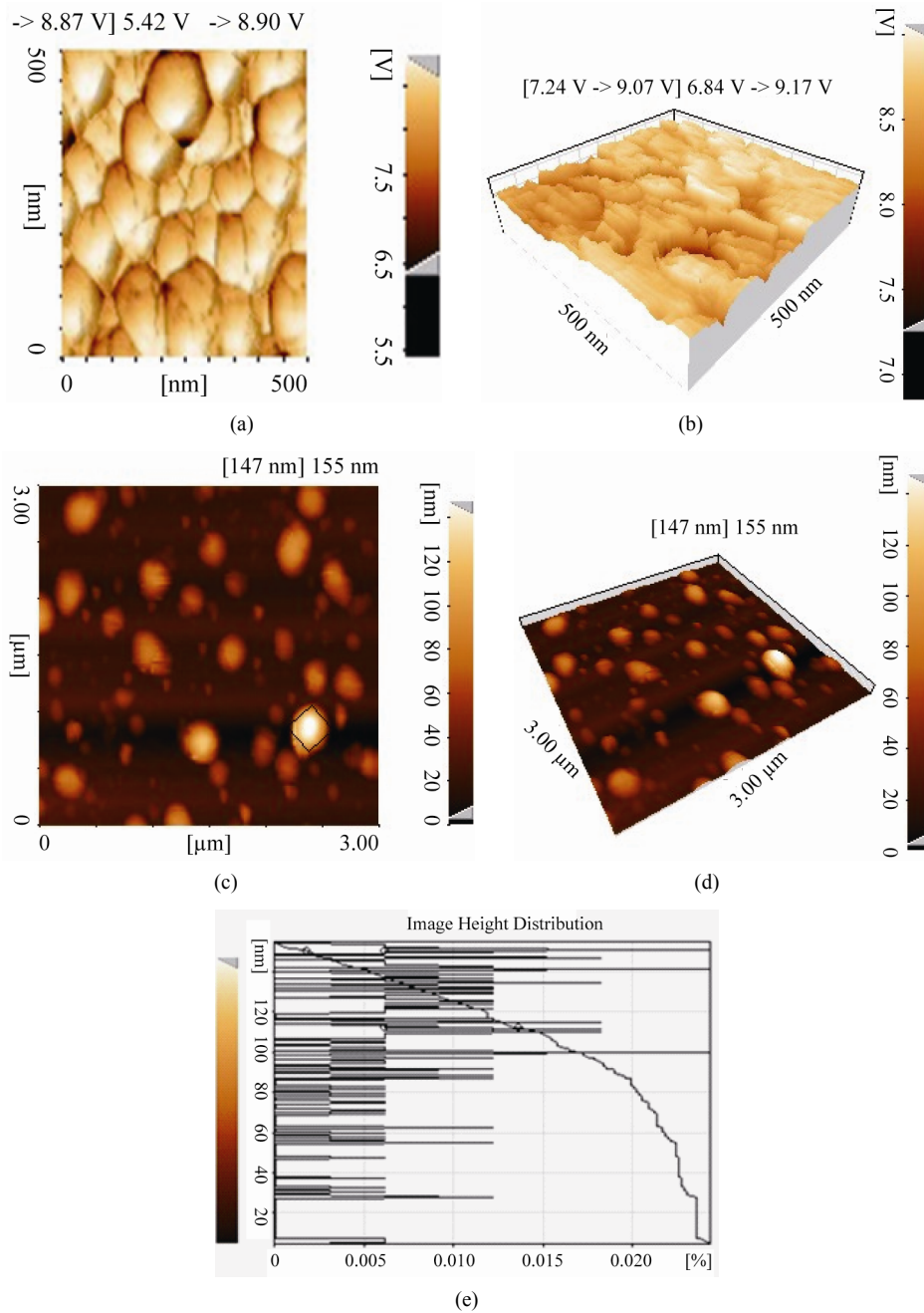


Figure 3. AFM photographs of surface topography of SiO₂, 2-D (a), SiO₂, 3-D (b), SiO₂/Au 2-D (c), SiO₂/Au 3-D (d) and height distribution (roughness) of SiO₂/Au nanoshells (e).

and ϵ_c , ϵ_m and ϵ_e the dielectric functions of the core, shell and embedding medium respectively where ϵ_c was taken to be 2.07 for the silica core at all wavelengths. μ

The values of complex dielectric function for gold at different wavelengths are obtained from Johnson and Christy [24,25] and the refractive index of the embedding medium of nanoshells i.e. water is taken as 1.50. However, the Drude model for the optical properties of a free electron model states that the real (ϵ_r) and imaginary

($j\epsilon_i$) parts of the dielectric function are [26,27]:

$$\epsilon_r = 1 - \frac{\omega_p^2}{\omega^2 + \gamma^2} \tag{12}$$

$$\epsilon_i = \frac{\omega_p^2 \gamma}{\omega(\omega^2 + \gamma^2)} \tag{13}$$

where ω_p is the plasma frequency, $\omega = 2\pi c/\lambda$, c the speed of light in a vacuum, λ the wavelength of incident light

and γ the damping constant. Decreasing the size of a nanoparticle will eventually cause the thickness to become less than the bulk mean free path, and electron scattering from the surfaces of the particle will have the effect of decreasing and broadening its plasmon resonance peak(s).

$$\gamma = \gamma_{bulk} + \frac{v_f}{r_{eff}} \quad (14)$$

where γ_{bulk} is the damping constant for the bulk material, v_f is the electron velocity at the Fermi surface and r_{eff} is effective mean free path of collisions. The latter can be

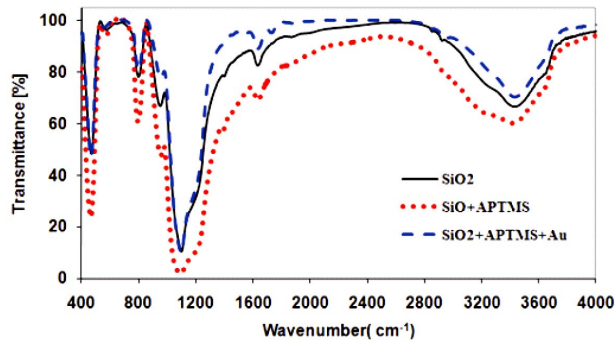


Figure 4. FTIR of SiO₂ functionalized with APTMS for sample A.

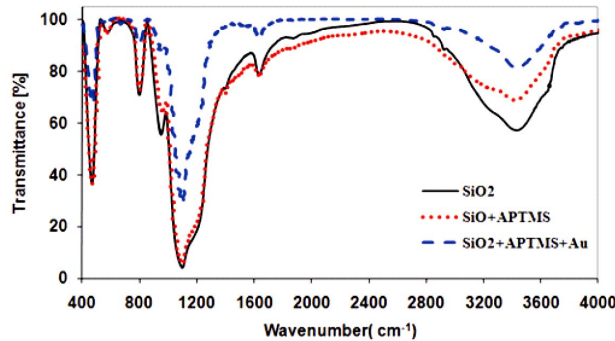


Figure 5. FTIR of SiO₂ functionalized with APTMS for sample B.

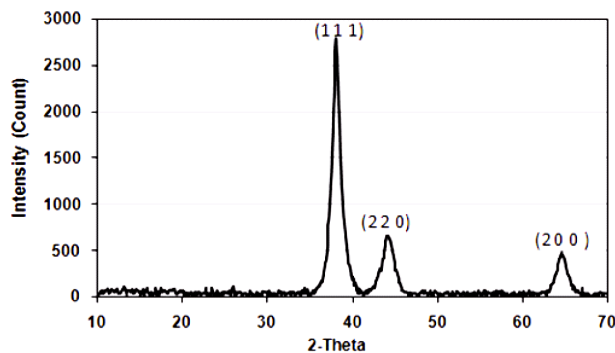


Figure 6. XRD spectra of gold nanoshells.

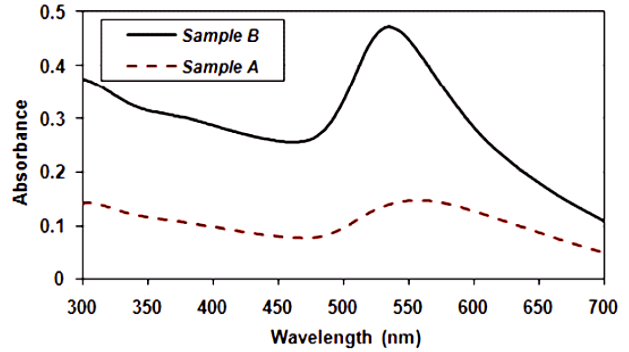


Figure 7. UV-visible spectroscopy of gold nanoshells synthesized by different amount of TEOS.

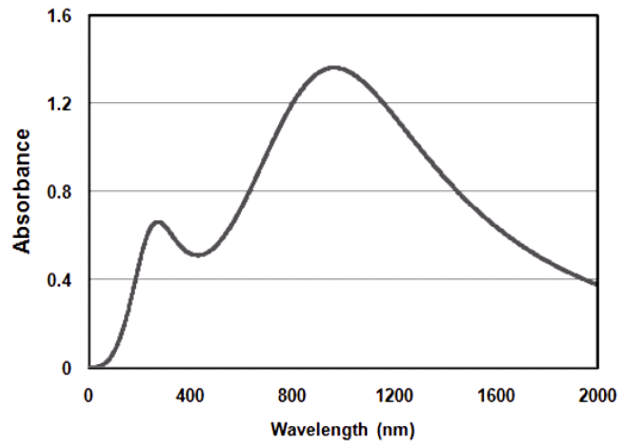


Figure 8. Calculated absorption spectra as a function of the wavelength.

calculated from [28]:

$$r_{eff} = \frac{\{(d_2 - d_1)(d_2^2 - d_1^2)\}^{\frac{1}{3}}}{2} \quad (15)$$

$$\epsilon_m = \epsilon_r + j\epsilon_i \quad (16)$$

$$P = 1 - (r_1 / r_2)^3 \quad (17)$$

$$\epsilon_a = \epsilon_c(3 - 2P) + 2\epsilon_m P \quad (18)$$

$$\epsilon_b = \epsilon_c P + \epsilon_m(3 - P) \quad (19)$$

The value of the dipole approximation resides in its ability give good estimation for the absorption and scattering properties of nanoshells, including the position of the resonant extinction peak. From Mie scattering theory, the absorption σ_{abs} and scattering σ_{sca} cross-sections are given by [29]:

$$\sigma_{sca} = \frac{8\pi^3}{3\epsilon_0^2 \lambda^4} |\alpha|^2, \quad \sigma_{abs} = \frac{2\pi}{\lambda \epsilon_0} \text{Im}(\alpha) \quad (20)$$

where λ is the wavelength and $\epsilon_0 = 8.85 \times 10^{-12} \text{ Fm}^{-1}$ is the free space permeability and $\text{Im}(\alpha)$ is the imaginary

part of complex polarizability of particle (α).

Resonance occur when dominator approaches zero. Therefore resonance wavelength depends on the ratio of core—shell radius as well as the material properties.

As it can be seen in **Figure 8** two peaks are observed at 250 and 1000 nm where the first one is related to HAuCl_4 [30,31] and the second peak represents the gold nanoshell with 100nm core diameter and 25 nm shell thickness.

4.6. Thermal Properties

To evaluate the surface plasmon-based photothermal effect of the synthesized nanostructure, variation of tissue temperature was plotted as a function of laser power density, see **Figure 9**. As it is seen not only the temperature increases with increasing the laser power density but also the temperature rise at constant power density is higher for higher gold concentration. This effectively indicates that higher gold concentration is accompanied with enhanced absorption cross section for spherical metal nanoparticles to achieve a better tissue soldering. Example of tissue before and after soldering at 60 W/cm^2 is shown in **Figure 10**. It is clearly seen that the incision is completely closed and there after it is expected that the wound repair process to take place.

5. Conclusions

Gold nanoshells were synthesized by Duff-Stober techniques and their chemical and optical properties were investigated. A variety of parameters can influence the

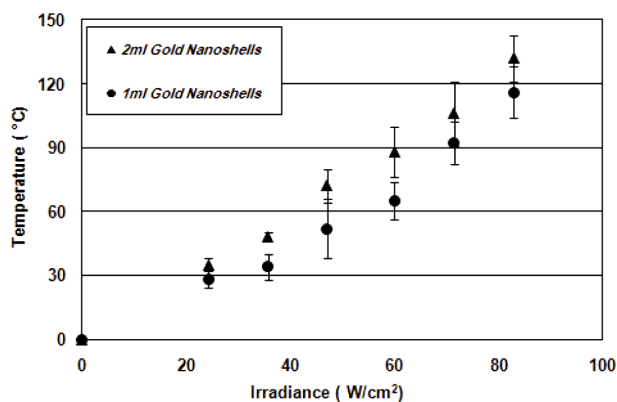


Figure 9. Variation of SiO_2/Au nanoshells temperature with laser power density for different concentrations.

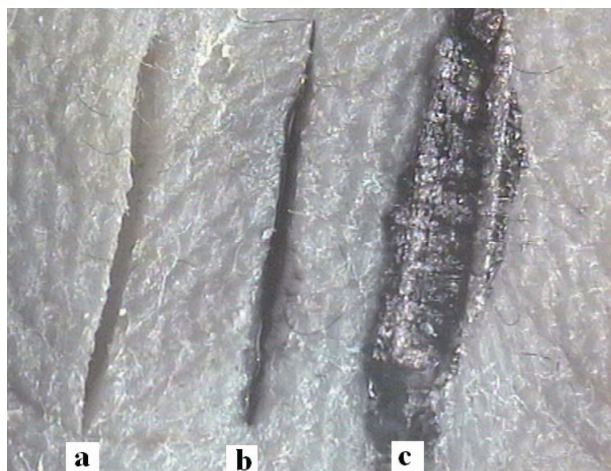


Figure 10. An example of skin tissue before and after laser soldering at $I = 60\text{W}/\text{cm}^2$. (a) Initial incision (b) Incision plus nanofluid before soldering and (c) incision after treatment.

self-assembly of gold nanoparticles into clusters attached to the surfaces of functionalized silica nanoparticles which in this case hydrophilic functional groups such as NH_2 led to the attachment of gold nanoparticles.

Smallest average size of silica was about 90 nm using 1 ml TEOS. Uv-vis spectroscopy demonstrated an absorption spectrum between 470 - 600 nm with a maximum peak at 550 nm which is different to experimental modelling result at about 1000 nm. This difference emphasizes the importance of size variation and shells random distribution in the laser wavelength selection for an appropriate application. The unique, tunable and strong optical responses of gold nanoshells are most desirable as exogenous agent for biophotonics applications. The core-shell morphology was also studied by AFM and based on SPR and Mie theory higher concentration of gold nanoparticles produced a higher temperature rise. A maximum measured tissue surface temperature due to SPR-induced thermal effect was about 130°C at $80\text{W}/\text{cm}^2$ using 2 ml SiO_2/Au nanoshells and diode laser. The preliminary result of possible laser tissue soldering employing core-metal shell is demonstrated and can further be developed provided the physics and biophysics behind is understood and clarified.

6. References

- [1] G. Mie, "Contributions to the Optics of Turbid Media, Particularly of Colloidal Metal Solutions," *Annals of Physics*, Vol. 25, No.3, 1908, pp. 377-445.
[doi:10.1002/andp.19083300302](https://doi.org/10.1002/andp.19083300302)

$$\alpha = \varepsilon_0 \frac{(\varepsilon_m - \varepsilon_e)(\varepsilon_c + 2\varepsilon_m) + (R_c / R_m)^3 (\varepsilon_c - \varepsilon_m)(\varepsilon_e + 2\varepsilon_m)}{(\varepsilon_m + 2\varepsilon_e)(\varepsilon_c + 2\varepsilon_m) + (R_c / R_m)^3 (\varepsilon_c - \varepsilon_m)(2\varepsilon_m - \varepsilon_e)} 4\pi R_m^3 \quad (21)$$

- [2] S. R. Sershen, S. L. Wescott, J. L. West and N. J. Halas, "An Opto-Mechanical Nanoshell-Polymer Composite," *Applied Physics B*, Vol. 73, No.4, 2001, pp. 379-381. [doi:10.1007/s003400100689](https://doi.org/10.1007/s003400100689)
- [3] A. O. Pinchuk and G. C. Schatz, "Collective Surface Plasmon Resonance Coupling in Silver Nanoshell Arrays," *Applied Physics B*, Vol. 93, No. 1, 2008, pp. 31-38. [doi:10.1007/s00340-008-3148-6](https://doi.org/10.1007/s00340-008-3148-6)
- [4] C. Loo, A. Lin, L. Hirsch, M. Lee and N. Halas, "Nanoshell-Enabled Photonics-Based Imaging and Therapy of Cancer," *Technology in Cancer Research and Treatment*, Vol. 3, No. 1, 2004, pp. 33-40.
- [5] A. Schwartzberg, T. Y. Olson, C. Talley and J. Z. Zhang "Synthesis, Characterization and Tunable Optical Properties of Hollow Gold Nanospheres," *Journal of Physical Chemistry B*, Vol. 110, No. 40, 2006, pp. 19935-19944. [doi:10.1021/jp062136a](https://doi.org/10.1021/jp062136a)
- [6] J. Eastman, S. Phillpot, S. Choi and P. Kelbinski, "Thermal Transport in Nanofluids," *Annual Review of Materials Research*, Vol. 34, 2004, pp. 219-246.
- [7] P. Kelbinski, R. Prasher and J. Eapen, "Thermal Conductance of Nanofluids: Is the Controversy Over?" *Journal of Nanoparticle Research*, Vol. 10, No. 7, 2008, pp. 1089-1097. [doi:10.1007/s11051-007-9352-1](https://doi.org/10.1007/s11051-007-9352-1)
- [8] Y. Xuan, Q. Li and W. Hu, "Aggregation Structure and Thermal Conductivity of Nanofluids," *AICHE Journal*, Vol. 49, No.4, 2003, pp. 1038-1043. [doi:10.1002/aic.690490420](https://doi.org/10.1002/aic.690490420)
- [9] V. Shalaev and S. Kawata, "Nanophotonics with Surface Plasmons," Elsevier Press, New York, 2006.
- [10] S. Kalele, S. W. Gosavi, J. Urban and S. K. Kulkarni, "Nanoshell Particles: Synthesis, Properties and Applications," *Current Science*, Vol. 91, No. 8, 2006, pp.1038-1052.
- [11] T. Ung, L. M. Liz-Marzan and P. Mulvaney, "Controlled Method for Silica Coating of Silver Colloids. Influence of Coating on the Rate of Chemical Reactions," *Langmuir*, Vol. 14, No. 14, 1998, pp. 3740-3748.
- [12] Y. P. He, S. Q. Wang, C. R. Li, Z. Y. Wu and B. S. Zou, "Synthesis and Characterization of Functionalized Silica-coated Fe₃O₄ Superparamagnetic Nanocrystals for Biological Applications," *Journal of Physics D: Applied Physics*, Vol. 38, No. 9, 2005, pp. 1342-1350. [doi:10.1088/0022-3727/38/9/003](https://doi.org/10.1088/0022-3727/38/9/003)
- [13] W. Stöber, A. Fink and E. Bohn. "Controlled Growth of Monodisperse Silica Spheres in the Micron Size Range," *Journal of Colloid Interface Science*, Vol. 26, No. 1, 1968, pp. 62-69. [doi:10.1016/0021-9797\(68\)90272-5](https://doi.org/10.1016/0021-9797(68)90272-5)
- [14] A. K. Gangopadhyay and A. Chakravorty, "Charge Transfer Spectra of Some Gold(III) Complexes," *Journal of Chemical Physics*, Vol. 35, No. 6, 1961, pp. 2206-2209. [doi:10.1063/1.1732233](https://doi.org/10.1063/1.1732233)
- [15] D. J. Wu and X. J. Liu, "Tunable Near-Infrared Optical Properties of Three-Layered Gold-Silica-Gold Nanoparticles," *Applied Physics B*, Vol. 97, No.1, 2009, pp. 193-197. [doi:10.1007/s00340-009-3432-0](https://doi.org/10.1007/s00340-009-3432-0)
- [16] A. Patra, E. Sominska, S. Ramesh and Y. Kolytyn "Sonochemical Preparation and Characterization of Eu₂O₃ and Tb₂O₃ Doped in and Coated on Silica and Alumina Nanoparticles," *Journal of Physical Chemistry B*, Vol. 103, No. 17, 1999, pp. 3361-3365. [doi:10.1021/jp9847661](https://doi.org/10.1021/jp9847661)
- [17] H. J. Feng, Y. Chen, F. Q. Tang and J. Ren, "Synthesis and Characterization of Monodispersed SiO₂/Y₂O₃:Eu³⁺ Core-Shell Submicrospheres," *Materials Letters*, Vol. 60, No. 6, 2006, p. 737. [doi:10.1016/j.matlet.2005.10.022](https://doi.org/10.1016/j.matlet.2005.10.022)
- [18] X. M. Liu, P. Y. Jia, J. Lin and G. Z. Li, "Monodisperse Spherical Core-Shell Structured SiO₂-CaTiO₃:Pr³⁺ Phosphors for Field Emission Displays," *Journal of Applied Physics*, Vol. 99, No. 12, 2006, pp. 124902-124909. [doi:10.1063/1.2204751](https://doi.org/10.1063/1.2204751)
- [19] J. Wiesner, A. Wokaun and H. Hoffmann, "Surface Enhanced Raman Spectroscopy (SERS) of Surfactants Adsorbed to Colloidal Particles," *Progress in Colloid and Polymer Science*, Vol. 76, 1988, pp. 271-277. [doi:10.1007/BFb0114205](https://doi.org/10.1007/BFb0114205)
- [20] S. Park, M. Park, P. Han and S. Lee, "Relative Contributions of Experimental Parameters to NIR-Absorption Spectra of Gold Nanoshells," *Journal of Industrial and Engineering Chemistry*, Vol. 13, No. 1, 2007, p. 65-70.
- [21] H. C. Lu, I. S. Tsai and Y. H. Lin, "Development of Near Infrared Responsive Material Based on Silica Encapsulated Gold Nanoparticles," *Journal of Physics: Conference Series*, Vol. 188, No. 1, 2009, Article ID: 012039.
- [22] R. D. Averitt, S. L. Westcott and N. J. Halas, "Ultrafast Electron Dynamics in Gold Nanoshells," *Physical Review B*, Vol. 58, No. 16, 1998, pp. 10203-10206. [doi:10.1103/PhysRevB.58.R10203](https://doi.org/10.1103/PhysRevB.58.R10203)
- [23] A. Vial, A. S. Grimault, D. Barchiesi and M. L. de la Chapelle, "Improved Analytical Fit of Gold Dispersion: Application to the Modeling of Extinction Spectra with a Finite-Difference Time-Domain Method," *Physical Review B*, Vol. 71, No. 8, 2005, pp. 85416-85423
- [24] P. B. Johnson and R. W. Christy, "Optical Constants of the Noble Metals," *Physical Review B*, Vol. 6, No. 12, 1972, pp. 4370-4379. [doi:10.1103/PhysRevB.6.4370](https://doi.org/10.1103/PhysRevB.6.4370)
- [25] S. Srivastava, M. Haridas and J. K. Basu, "Optical Properties of Polymer Nanocomposites," *Bulletin of Material Science*, Vol. 31, No. 3, 2008, pp. 213-218. [doi:10.1007/s12034-008-0038-9](https://doi.org/10.1007/s12034-008-0038-9)
- [26] C. F. Bohren and D. R. Huffman, "Absorption and Scattering of Light by Small Particles," Wiley Press, Boston, 1998.
- [27] M. Bass, C. Decusatis, G. Li, V. Lakshminarayanan, E. Van Stryland and V. N. Mahajan, "Optical Properties of Materials," *Handbook of Optics*, 3rd Edition, Vol. 4, McGraw Hill Professional Press, Boston, 2009.
- [28] P. Mulvaney, "Surface Plasmon Spectroscopy of Nanosized Metal Particles," *Langmuir*, Vol. 12, No. 3, 1996, pp. 788-800.
- [29] P. N. Njoki, I. S. Lim, D. Mott, H. Y. Park, B. Khan, S. Mishra, R. Sujakumar, J. Luo and C. J. Zhong, "Size Correlation of Optical and Spectroscopic Properties for Gold

- Nanoparticles,” *Journal of Physical Chemistry C*, Vol. 111, No. 40, 2007, pp. 14664-14669.
[doi:10.1021/jp074902z](https://doi.org/10.1021/jp074902z)
- [30] R. D. Badly, W. T. Ford, F. J. MacEnroe and R. A. Assink, “Surface Modification of Colloidal Silica,” *Langmuir*, Vol. 6, No. 4, 1990, pp. 792-801.
- [31] A. Vogler and H. Kunkely, “Photoreactivity of Gold Complexes,” *Coordination Chemistry Reviews*, Vol. 219-221, 2001, pp. 489-507.